



Universitat de Lleida

Document downloaded from:

<http://hdl.handle.net/10459.1/70129>

The final publication is available at:

<https://doi.org/10.1039/D0EN00110D>

Copyright

(c) Royal Society of Chemistry, 2020

Stable Zn isotopes reveal the uptake and toxicity of zinc oxide engineered nanomaterials in *Phragmites australis*

Caldelas C^{1*}, Poitrasson F², Viers J², and Araus JL^{1,3}.

¹Department of Evolutive Biology, Ecology, and Environmental Sciences. University of Barcelona. Av. Diagonal, 643, 08015, Barcelona, Spain.

Cristina Caldelas*, (+34) 657345950, criscaldelas@ub.edu

José Luis Araus, (+34) 934021469 jaraus@ub.edu

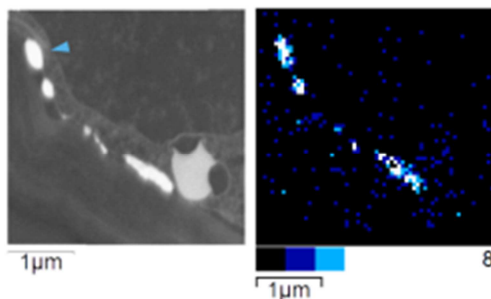
²Géosciences Environnement Toulouse, UMR 5563 Centre National de la Recherche Scientifique - Université de Toulouse - Institut de Recherches pour le Développement, 14-16, avenue Edouard Belin, 31400, Toulouse, France.

³AGROTECNIO Center, University of Lleida, 25198 Lleida, Spain

Franck Poitrasson, +33 (0)561332619, Franck.Poitrasson@get.omp.eu

Jérôme Viers, +33 (0)0561332624, jerome.viers@get.omp.eu

Table of contents



The Zn stable isotope composition of plants demonstrates that ZnO engineered nanomaterials dissolve before their uptake and accumulation by the roots (brightest inclusions in root cortex above).

Abstract

The uptake, transport, and toxicity mechanisms of zinc oxide (ZnO) engineered nanomaterials (ZnO-ENMs) in aquatic plants remain obscure. We investigated ZnO-ENM uptake and phytotoxicity in *Phragmites australis* by combining Zn stable isotopes and microanalysis. Plants were exposed to four ZnO materials: micron-size ZnO, nanoparticles (NPs) of <100 nm or <50 nm, and nanowires of 50 nm diameter at concentrations of 0-1000 mg l⁻¹. All ZnO materials reduced growth, chlorophyll content, photosynthetic efficiency, and transpiration and led to Zn precipitation outside the plasma membranes of root cells. Nanoparticles <50 nm released more Zn²⁺ and were more toxic, thus causing greater Zn precipitation and accumulation in the roots and reducing Zn isotopic fractionation during Zn uptake. However, fractionation by the shoots was similar for all treatments and was consistent with Zn²⁺ being the main form transported to the shoots. Stable Zn isotopes are useful to trace ZnO-ENM uptake and toxicity in plants.

Environmental Significance Statement

Our understanding of zinc oxide nanomaterials interaction with wetland plants is hampered by the lack of scientific consensus about their uptake and toxicity mechanisms in these species. This is a serious concern given the alarming global increase in the discharge of these nanomaterials into the environment and the key ecological roles of wetland plants. The Zn isotopic signature of plant tissue integrates all the Zn metabolic pathway throughout the plant's life, giving insight about the form of Zn taken up, even if this later transforms into another Zn species. Thus, our findings clarify the exposure routes and the mechanisms of action of zinc oxide engineered nanomaterials in wetland plants while advancing the toolbox for plant physiology and environmental studies.

Introduction

An estimated 34,000 tonnes year⁻¹ of ZnO-ENMs are emitted into the environment globally, of which 3,000 are directly discharged into water bodies¹. Models predict that sediments will receive most of the ZnO-ENMs released into water bodies (up to 1 mg Kg⁻¹ year⁻¹)², especially near large cities and related industry, in areas that favour deposition like wetlands and marshes. This may cause chronic toxicity in emergent wetland plants (helophytes), which play vital ecological roles³. Exposure to ZnO-ENMs decreases photosynthesis, antioxidant activity, and growth in aquatic plants, and increases Zn bioaccumulation and oxidative stress⁴⁻¹⁰. However, studies on helophytes are few and the uptake and toxicity of ZnO-ENMs, especially after chronic exposure, are poorly characterised in these plants.

There is an unresolved controversy about the capacity of entire ZnO-ENMs to enter roots. In several crops, ZnO-ENMs have been reported in the root epidermis, cortex, endodermis, stele, lateral roots, and on the root surface¹¹⁻¹⁶. At the cellular level, ZnO-ENMs have accumulated in the intercellular spaces, along the plasma membrane, and in the cytoplasm, vacuoles and nuclei^{11,14}. It has been suggested that ZnO-ENMs in the root apoplast can enter the symplast by endocytosis¹¹ and pass to the xylem directly from the apoplast, through lateral roots with immature Casparian bands^{6,14}. However, few studies have confirmed either the elemental composition of the candidate ENMs or the Zn speciation in roots. Wang *et al* found 65% ZnO and 32% Zn-histidine in the roots of hydroponically grown cowpea exposed to ZnO-ENMs¹². Nonetheless, Da Cruz *et al* demonstrated that ZnO was only found inside roots when they had been previously damaged¹³. Accordingly, ZnO-ENMs normally do not reach the shoots unless roots are damaged¹²⁻¹⁵. Intact roots generally contain no ZnO but do contain other Zn species like Zn-phosphates, Zn-citrate, Zn-malate, Zn-histidine, or Zn-nitrate^{13,14,16}. In the aquatic plant *Schoenoplectus tabernaemontani*, ZnO-ENMs were reportedly found around plastids in the roots, arranged like beads on a string⁶. However, this observation could be better explained as endoplasmic reticulum wrapped around plastids¹⁷.

The present research aims to give a comprehensive insight on ZnO-ENM uptake and chronic toxicity in *P. australis* at the levels estimated by models in current sediments, with an ample margin for a future increase in concentrations. This is crucial because emissions are expected to continue growing. To do so, we determined whether entire ZnO-ENMs enter *P. australis* roots by combining transmission electron microscopy (TEM), X-ray microanalysis, dark-field mapping, and Zn stable isotope analysis in different plant organs. Zinc stable isotopes are valuable to understand Zn uptake and toxicity in plants^{18,19}. The Zn isotopic signature of plant tissue integrates all the processes causing Zn fractionation throughout a plant's life and it is a proxy of Zn speciation and the activity of Zn membrane transporters²⁰. Hence, Zn isotopes can be used to determine whether Zn was first taken up as either Zn²⁺ or ZnO-ENMs, even after they form other Zn species. Additionally, we unravelled the mechanisms of ZnO-ENM toxicity on the photosynthetic apparatus and fully characterised the physiological response of *P. australis* to ZnO-ENMs.

Methods

Nanomaterials and non-nano ZnO

Four ZnO materials were purchased from Sigma-Aldrich: non-nano ZnO (96479 Fluka, ACS reagent $\geq 99.9\%$); spherical particle nanopowder <100 nm in diameter (544906 Aldrich, $\approx 80\%$); <50 nm nanopowder particles of various shapes (677450 Aldrich, $>97\%$); and nanowires 50 nm in diameter x 300 nm long (773980 Aldrich). These materials will be referred to as Bulk, NP100, NP50, and NW, respectively. To determine their chemical composition, 2 ml HNO₃ (69.0-70.0% Instra reagent, 9598-34 Baker) was added to 50 mg aliquots and digested overnight at 90°C. The extracts were brought to 100 ml with 1% HNO₃ and analysed for Al, Cd, Cr, Cu, Fe, Ni, Pb, and Zn content by inductively coupled plasma optical emission spectrometry (ICP-OES) using a Perkin Elmer Optima-8300 (Waltham, MA, USA). Three replicates were analysed for each ZnO material. To study particle size and shape, samples were observed on a field

emission scanning electron microscope (FESEM) JEOL JSM 7100F at 20.0 kV, and secondary electron images were taken.

Plant growth conditions

Phragmites australis (Cav.) Trin. Ex Steud plants were purchased from a local nursery (Tres Turons, Sabadell, Spain). Plant cultivation took place in the greenhouse of the Experimental Field Services of the University of Barcelona (UB). Roots were washed to remove the original substrate and shoots cut to induce new growth. Plants were initially grown in trays filled with modified half-strength Hoagland's solution as detailed in¹⁸. The pH was adjusted to 6.5 and solution was replaced every three days. After 7 weeks, plants were rinsed in distilled water, selected within a small range of fresh weight (11.99 ± 0.23 g, mean \pm standard error, $n = 95$) and height (27.54 ± 0.34 cm), and placed in individual 1-gallon (3.895 l) glass pots. These were filled with modified half-strength Hoagland's solution with no added Zn according to²¹ (Supplementary Table 1), at pH 5.9. Each pot was wrapped in aluminium foil to limit algal growth. After 10 days, the ZnO materials described above were added at a concentration of 0, 0.1, 1, 10, 100, or 1000 mg l⁻¹. Nanowires were only tested up to 10 mg l⁻¹ due to their high cost. Four pots per treatment were distributed randomly on the greenhouse table, and the nutrient solution was replenished three times a week. Five pots without plants but containing the same solution were included. Plants were grown for 14 weeks, from November 2016 to February 2017. The mean temperature was $17.9 \pm 0.22^\circ\text{C}$, the relative humidity $51.0 \pm 1.06\%$, and the maximum PPFD (photosynthetic photon flux density) $\sim 500 \mu\text{mol m}^{-2} \text{s}^{-1}$. The pH and electrical conductivity (EC) of the solutions were controlled weekly in a sub-sample of 10 pots (results not shown) and recorded for the whole experiment on weeks 8 and 12 (Supplementary Table 2).

Elemental analyses

At the end of the experiment, 10 ml aliquots of the growth solutions were centrifuged for 10 minutes at 9065 relative centrifugal force in a Hettich 32R centrifuge (Tuttlingen, Germany) with a 1620A angle rotor. Supernatants were filtered using Whatman® Grade GF/A glass

microfibre filters (WHA1820042) and 100 µl HNO₃ was added (Baker Instra-Analysed Reagent, 69.0-70.0%, 9598-34). The Zn and Al contents of the solutions were measured by ICP-OES.

Plants were thoroughly washed in distilled water, patted dry, and weighed. Roots and shoots were separated using a scalpel. Samples were oven-dried at 60°C for 48h and finely ground for 2 min in a Retzch MM400 mixer mill at a frequency of 20 s⁻¹. Next, 0.1 g of the ground material was digested overnight at 90°C in a mixture of 2 ml HNO₃ and 0.5 ml H₂O₂ (30% Suprapur, 1.07298.1000 Merck). Then 50 µl of HF (40% reagent grade, AC10511000 Scharlab) were added to each sample and digested for an additional 2h at 90°C. Digests were diluted in 30 ml MilliQ water (18.2 Ω) before analysis. Per every 30 samples, 3 blanks and 2 aliquots of the BCR-60 reference material (*Lagarosiphon major*) (Community Bureau of Reference, Brussels, Belgium) were digested using the same protocol. We obtained 303.1±5.3 (n=6) µg g⁻¹ Zn, in line with the certified values (313.0±8.0). The Al, Ca, Cu, Fe, K, Mg, Mn, P, S, and Zn contents of the extracts were then determined by ICP-OES. To study Zn mass balance at the end of the experiment, Zn in mg was calculated for each reservoir in our culture system (Equation 1):

$$Zn_{\text{watering}} + Zn_{\text{ZnO}} = Zn_{\text{root}} + Zn_{\text{shoot}} + Zn_{\text{solution}} + Zn_{\text{solid}}$$

The Zn input contributed by the nutrient solution (Zn_{watering}) was calculated by multiplying the [Zn] of the initial nutrient solution by the total volume of solution added and by the sum of all waterings (E). Zinc input from ZnO materials (Zn_{ZnO}) was obtained from the [ZnO] of each treatment (0.1, 1, 10, 100, and 1000 mg l⁻¹) multiplied by the Zn concentration of each material. Zinc extracted by roots (Zn_{root}) and shoots (Zn_{shoot}) was determined by multiplying [Zn] by dry weight (DW). The total Zn in the final solutions (Zn_{solution}) was calculated by multiplying [Zn] in the final solutions by the volume of the container. Finally, the Zn in the solid phase of the nutrient media (Zn_{solid}) was inferred from subtracting Zn_{root} , Zn_{shoot} , and Zn_{solution} from the sum of all Zn inputs. The same procedure was followed to calculate the Al mass balance.

Zinc separation and isotopic analyses

Zinc isotope analyses were carried out in the facilities of the Géosciences Environnement, Toulouse, France. In the clean lab (ISO3), 100 mg of sample were weighed in Teflon beakers. Samples were digested in several steps: i) 24h at room temperature in 1.5ml HNO₃ and 1 ml H₂O₂; ii) 24h on a hotplate at 80°C with the same mixture, then evaporated; iii) 24h at 80°C in a mixture of 1.2ml HF and 1.2 ml HNO₃, then evaporated; and finally iv) 24h on a hotplate at 115°C in 20 drops of HCl and 10 drops of HNO₃, and evaporated. The digests were then refluxed in 15 ml 10% HNO₃ for Zn quantification in an ICP-MS Agilent 7500 (Santa Clara, USA). Three aliquots of BCR-60 were ground and processed in the same manner as the samples to quantify the Zn contribution of the stainless-steel jars and balls. We obtained 298.2±2.1 µg g⁻¹ ⁶⁶Zn for the ground BCR-60 and 301.3±6.9 for the non-ground. These values are slightly lower than the certified 313.0±8.0 µg g⁻¹ Zn, which is likely due to the cleanroom being a much cleaner environment than a regular chemistry laboratory. The sample residual was weighed and refluxed in 1 ml of 7N HCl + 0.001% H₂O₂ overnight at 40°C. HCl and HNO₃ were double distilled, HF was 41-51% (Fluka A513-P500 suprapur) and H₂O₂ 30% (Merk 1.07298 suprapur). Plastic and Teflon material was acid-washed before use. Zinc separation was performed in Poly-Prep chromatography columns (BIO-RAD, 731-1550) containing 2 ml of anion exchange resin AGMP-1M (100-200 mesh, chloride form) (BIO-RAD, 1411841). The resin was first cleansed three times with 10 ml 18.2Ω water followed by 7 ml 0.5N HNO₃, then conditioned with 6 ml 7N HCl + 0.001% H₂O₂ before loading the samples. Matrix elements and Cu were eluted with 30 ml 7N HCl + 0.001% H₂O₂. Iron (Fe) was eluted with 10 ml 2N HCl + 0.001% H₂O₂ and the resin was rinsed in 2 ml of 0.5N HNO₃. Finally, Zn fractions were eluted on 8 ml of 0.5N HNO₃ and evaporated. Three aliquots of the reference material BCR 281 (ryegrass) were processed in the same manner to check the accuracy of the isotope measurements. Digested ZnO materials were diluted up to 1:3000. Column yield was checked from the Zn intensities during isotope analysis and was 96.6 ± 18.0 % (mean ± 2SD, n=48) for plant samples and 89.7 ± 5.6 (n=12) for ZnO materials. Three samples with bad yields were rejected and were not included in this study. Zinc fractions were concentration-matched to

within 10% and measured for Zn isotopic composition in a High-Resolution Multi-Collector ICP Mass Spectrometer (Neptune, ThermoFinnigan). Instrument settings are shown in Supplementary Table 3. The Neptune cup configuration was: L4 (^{62}Ni), L2 (^{63}Cu), L1 (^{64}Zn), Central (^{64}Cu), H1 (^{66}Zn), H2 (^{67}Zn), and H3 (^{68}Zn). To correct for mass bias, the sample-standard bracketing procedure as described in²² was applied, with AA ETH Zn as bracketing standard and copper (Cu) NIST SRM 976 as the external element. Sample and standard measurements were obtained from 40 cycles of 8-second integrations. Samples were measured 2-3 times on different sessions. Repeatability throughout the three sessions was $0.002\text{‰} \pm 0.035$ (2SD; $n = 150$), calculated from the bracketing standard. Isotope compositions are expressed in the δ notation (Equation 2):

$$\delta X = \left(\left(\frac{R_s}{R_{st}} \right) - 1 \right) \times 1000$$

For a given chemical element (X), R_s is the ratio of the heavy isotope to the light isotope of the sample and R_{st} of the standard. All $\delta^{66}\text{Zn}$ in this study were calculated using the 66 and 64 isotopes and expressed relative to JMC Zn. The $\delta^{66}\text{Zn}_{\text{JMC}}$ for AA ETH Zn and ryegrass were 0.27 ± 0.04 (2SD; $n = 150$), and 0.42 ± 0.06 (2SD; $n = 6$) respectively, which was in agreement with the literature^{23,24}.

Root anatomy and root cell ultrastructure

Root tips were cut from controls and plants treated with either 1000 mg l^{-1} (Bulk, NP100, NP50) or 10 mg l^{-1} (NW) for 9 weeks. Root tips were rinsed in distilled water and fixed in an ice-cold mixture of 2.5% glutaraldehyde and 2% paraformaldehyde in 0.1M phosphate buffer (pH 7.4), then stored at 4°C . Samples were exposed to vacuum for 1h to remove air bubbles, washed in phosphate buffer, and postfixed and stained with 1% osmium tetroxide and 0.8% potassium ferrocyanide for 1h. Stained samples were washed in distilled water and dehydrated in an acetone series of increasing concentration to achieve 100%. All the fixation steps were carried out at 4°C . Fixed samples were polymerised in epoxy Spurr resin for 48h at 60°C . For light microscopy, $1 \mu\text{m}$ semi-thin cross-sections were stained with methylene blue and photographed

with a light microscope (Olympus 175 CX41, Tokyo, Japan) coupled with a digital camera (Olympus DP70). For transmission electron microscopy (TEM), 70 nm ultrathin sections were cut with a Reichert-Jung Ultracut E ultramicrotome (C. Reichert AG, Vienna, Austria), stained with uranyl acetate and lead citrate, and observed under a Jeol JEM 1010 (Tokyo, Japan) operated at 100 kV. Images were taken with a Gatan Orius camera (Gatan, Pleasanton, USA). For microanalysis, unstained cuts were dried and mounted on titanium grids. Cuts were analysed using a JEOL JEM-2100 LaB6 transmission electron microscope equipped with an Energy Dispersed Analysis of X-ray Spectrometer (EDXS), operating at 200 kV in STEM mode using the dark field detector. The beam size used in this mode was around 15 nm. The spectrometer is an INCA x-sight (Oxford Instruments, Abingdon, UK), with a Si (Li) detector. Micrographs were obtained using a Gatan Orius SC1000 CCD camera with Digital Micrograph Version 1.71.38 software. Map acquisition was accomplished using the INCA Microanalysis Suite version 4.09 software. X-ray maps were obtained by selecting Zn $\text{K}\alpha 1$ as the characteristic X-ray peak.

Evapotranspiration and photosynthetic performance

To calculate the water consumption from each pot (E, in g), the nutrient solution added during each watering was weighed. Chlorophyll content on a leaf area basis was measured with a SPAD-502 portable chlorophyll meter (Minolta, Illinois, USA), as reported elsewhere²⁵. Five representative mature leaves of each plant were measured at 2 cm from the base. The leaf gas exchange and chlorophyll fluorescence were determined using a Li-COR 6400 portable photosynthesis system (Li-COR Inc., Lincoln, NE, USA) running OPEN version 4.06. The third fully developed leaf of the healthiest shoot of each plant was measured at approximately 2 cm from the base. Leaves were first dark-adapted for 30 min to measure maximum quantum yield (F_v/F_m). The same leaves were then re-acclimated to environmental light until stabilised (up to 45 min) to determine relative quantum yield (F_v'/F_m'), quantum yield of photosystem-II photochemistry (ΦPSII)²⁶, quantum yield of CO_2 fixation (ΦCO_2), the electron transport rate (ETR, $\mu\text{mol m}^{-2}\text{s}^{-1}$), photochemical (qP) and non-photochemical quenching (qN, NPQ), the

light-saturated net CO₂ assimilation rate (A_s , $\mu\text{mol CO}_2 \text{ m}^{-2}\text{s}^{-1}$), stomatal conductance to water (g_s , $\text{mol H}_2\text{O m}^{-2}\text{s}^{-1}$), intercellular CO₂ concentration (C_i , $\mu\text{mol CO}_2 \text{ mol air}^{-1}$), the transpiration rate (E , $\text{mmol H}_2\text{O m}^{-2}\text{s}^{-1}$), and water vapour pressure deficit of the leaf (VPD, kPa).

Measurements were taken under a saturating light (photosynthetic photon flux density of 1200 $\mu\text{mol photons m}^{-2} \text{ s}^{-1}$), 400 $\mu\text{mol mol}^{-1}$ of CO₂, and an air temperature of $25.7 \pm 0.1^\circ\text{C}$.

Carbon and nitrogen isotopic relation in plants

For each plant sample, 0.8-0.9 mg of finely ground dry matter were weighed in tin capsules (Lüdiswiss, Flawil, Switzerland). The total C and N contents were analysed using an Elemental Analyser (EA, Carlo Erba 2100, Milan, Italy), which was interfaced with an Isotope Ratio Mass Spectrometer (IRMS, Thermo-Finnigan Deltaplus Advantage, Bremen, Germany) to analyse the $^{13}\text{C}/^{12}\text{C}$ and $^{15}\text{N}/^{14}\text{N}$ ratios. Results were expressed as $\delta^{13}\text{C}$ and $\delta^{15}\text{N}$ values following Eq. 2, using secondary standards calibrated against Vienna Pee Dee Belemnite calcium carbonate (VPDB) for C, and against N₂ air for N, respectively. Several certified reference materials were processed in the same manner, at a ratio of one aliquot each per 12 samples. For C, we used IAEA CH7 (measured $\delta^{13}\text{C}_{\text{VPDB}} -32.1 \pm 0.07\text{‰}$ on $n=15$, certified -32.2 ± 0.04); IAEA CH6 (measured -10.4 ± 0.08 on $n=15$, certified 10.5 ± 0.04), and USGS 40 (measured -26.5 ± 0.1 on $n=12$, certified -26.4 ± 0.04). For N, we analysed IAEA N1 (measured $\delta^{15}\text{N}_{\text{AIR}} 0.6 \pm 2.0\text{‰}$ on $n=14$, certified 0.4 ± 0.04), IAEA N2 (measured -20.3 ± 0.8 on $n=12$, certified 20.3 ± 0.07), IAEA NO3 (measured 4.7 ± 0.3 on $n=15$, certified 4.7 ± 0.2), and USGS 40 (measured -4.5 ± 0.3 on $n=11$, certified -4.5 ± 0.06).

Statistical methods

All the statistical analysis was done using R software version 3.4.0 for Windows. Analysis of variance (ANOVA) was performed on each variable based on a two-factor design with interactions. The differences between groups were assessed using paired-t-tests with Bonferroni correction (BF). When data did not meet the assumptions of equal variances or normality, the non-parametric Kruskal-Wallis (KW) ranks test and the Dunn's test with Benjamini-Hochberg

adjustment (Dunn) were used instead. Excel 2016 (Microsoft Office 365 Pro Plus version 1708) and Veusz 1.23.2 were used to create graphs.

Results

Characterisation of ZnO sources

Zinc purity was very similar in all four ZnO sources: 94.2% for Bulk, 96.3% for NP100, 90.2% for NP50, and 94.5% for NW (Supplementary Table 4). According to the manufacturer, Zn purity was 99.9%, ~80%, and 91% for Bulk, NP100, and NP50 respectively (no information was given for NW). Besides, 6% Al was reportedly added to NP50 as a dopant but only 2.2% was measured. Traces of other unreported elements were also found: up to 27.2 $\mu\text{g g}^{-1}$ Pb (NP50), 8.5 $\mu\text{g g}^{-1}$ Fe, 4.5 $\mu\text{g g}^{-1}$ Cu, 3.4 $\mu\text{g g}^{-1}$ Ni, 1.2 $\mu\text{g g}^{-1}$ Cd, and 0.7 $\mu\text{g g}^{-1}$ Cr. Average particle length was 215 ± 4 nm (mean \pm SE, $n = 946$) for bulk ZnO, with 10% of particles in the nano range. For NP100, the mean particle length was 99 ± 2 nm ($n = 956$), but 35% of the particles were >100 nm. Similarly, NP50 diameter was 48.7 ± 0.57 nm ($n = 467$), with 39% of the particles in the 50-100 nm range. Finally, the mean diameter of NW was 59 ± 0.5 nm ($n = 223$).

Zinc and Al dissolution and uptake

Zinc concentrations in the growth solution ($[\text{Zn}]_{\text{sol}}$), roots ($[\text{Zn}]_{\text{root}}$), and shoots ($[\text{Zn}]_{\text{shoot}}$) increased with increasing ZnO supply (Fig. 1, Supplementary Table 5), reaching 20x, 231x, and 60x those of the controls at 1000 mg l^{-1} , respectively ($P < 0.001$). Controls had similar $[\text{Zn}]_{\text{root}}$ and $[\text{Zn}]_{\text{shoot}}$ ($\sim 30 \mu\text{g g}^{-1}$). By contrast, plants treated with ZnO accumulated Zn preferentially in the roots (7.6 mg g^{-1} in roots vs. 1.8 mg g^{-1} in shoots at the highest ZnO supply) (Fig. 1B, C). At 100 and 1000 mg l^{-1} , NP50 released up to twice as much Zn into solution as bulk and NP100 ($P = 0.019$ and 0.011, respectively) (Fig. 1A). $[\text{Zn}]_{\text{shoot}}$ in plants treated with 1000 mg l^{-1} NP50 reached 3.1 mg g^{-1} , twice as much as bulk and NP100 plants ($P = 0.034$) (Fig. 1C), and $[\text{Zn}]_{\text{root}}$ reached 10.4 mg g^{-1} Zn, 60% higher than bulk and 80% higher than NP100 plants (Fig. 1B). The

mass balance was calculated to assess the fate of Zn in our system. The proportion of Zn in the solid fraction at the end of the experiment (Zn_{solid}) increased with increasing $[ZnO]$ ($P<0.001$) (Fig. 2). At 100 and 1000 $mg\ l^{-1}$, the majority of Zn (85 - 99 %) remained in the solid fraction. By contrast, the dissolved Zn fraction (Zn_{sol}) decreased with increasing ZnO ($P<0.001$). The fraction of Zn stored in roots (Zn_{root}) and shoots (Zn_{shoot}) gradually increased up to 10 $mg\ l^{-1}$ and decreased at the two highest concentrations ($P<0.001$). At 100 and 1000 $mg\ l^{-1}$, Zn_{sol} was the highest in NP50 treatments (9.8 and 2.9%, respectively). The maximum Zn_{root} was 16% and Zn_{shoot} 8%, both at 10 $mg\ l^{-1}$ NP50.

To study the uptake of doping elements by plants and the capacity of ENMs to retain metals from solution, Al content and mass balance were investigated. At 1000 $mg\ l^{-1}$ ZnO ($P<0.001$) (Supplementary Table 5) the $[Al]_{roots}$ was 3.5x higher than the control. The only Al-doped material, NP50, resulted in the highest $[Al]_{root}$ (up to 195 $mg\ g^{-1}$ at 1000 $mg\ l^{-1}$, $P=0.022$). The $[Al]_{shoots}$ increased from the 10 $mg\ l^{-1}$ ZnO treatments and beyond, with a maximum increase of 30% at 1000 $mg\ l^{-1}$ ZnO (all $P<0.001$). However, the mass balance calculations indicated that the Al missing from solution mostly ended up in the solid fraction (Al_{solid}), which increased progressively with $[ZnO]$ ($P<0.001$) (Supplementary Fig. 1). NP50 showed the highest Al_{solid} ($P<0.001$, Supplementary Fig. 1C), starting with 98.9% at 0.1 $mg\ l^{-1}$. For the rest of the ZnO materials, at 10 $mg\ l^{-1}$ the Al_{solid} was 42% in Bulk (Supplementary Fig. 1A), 59% in NP100 (Supplementary Fig. 1B), and 78% in NW (Supplementary Fig. 1D). The solution pH progressively increased in pots containing plants, reaching 8.2 by the end of the experiment, while pots without plants had a pH value of 5.5. At week 8, the pH of the 1000 $mg\ l^{-1}$ solutions was 1 pH unit higher than controls and close to neutrality ($P<0.001$) (Supplementary Table 2). The pH was highest in NP100 treatments and lowest with NW ($P=0.011$). At the end of the experiment, the solution pH was higher for plants under 1000 $mg\ l^{-1}$ ZnO and controls than for the rest of concentrations, with no difference between sources.

Zn isotopic fractionation

The $\delta^{66}\text{Zn}$ of all ZnO materials was very similar, on average $0.33 \pm 0.04 \text{ ‰}$ ($n = 10$, Fig. 3, Supplementary Table 6). By contrast, the $\delta^{66}\text{Zn}_{\text{root}}$ showed clear differences between treatments ($P=0.003$). Bulk and NP100 plants had the lightest $\delta^{66}\text{Zn}_{\text{root}}$ (0.02 and $0.04 \text{ ‰}^{\text{a}}$, respectively), followed by NP50 ($0.13 \text{ ‰}^{\text{ab}}$), and NW and controls (0.35 and $0.38 \text{ ‰}^{\text{b}}$, respectively). The $\delta^{66}\text{Zn}_{\text{shoot}}$ also differed between ZnO treatments ($P=0.027$, Fig. 3). The shoots of plants treated with bulk ZnO had the lightest $\delta^{66}\text{Zn}_{\text{shoot}}$ ($-0.61 \text{ ‰}^{\text{a}}$), while the rest of the ZnO treatments ranged -0.5 to $-0.32 \text{ ‰}^{\text{ab}}$, and controls had the heaviest $\delta^{66}\text{Zn}_{\text{shoot}}$ ($0.27 \text{ ‰}^{\text{b}}$). The root-to-shoot fractionation ($\Delta\text{Zn}_{\text{shoot-root}}$) was very small in controls (-0.08 ‰), which had no Zn added to the nutrient solution. For the rest of the treatments, $\Delta\text{Zn}_{\text{shoot-root}}$ ranged from -0.71 to -0.52 ‰ , with no statistically significant difference among them.

Plant growth and evapotranspiration

ZnO caused severe, dose-dependent effects on plant growth and evapotranspiration (ET). Fresh weight (FW) was reduced by up to 74% in whole plants, 66% in roots, and 88% in shoots, whereas $\text{FW}_{\text{root}}/\text{FW}_{\text{shoot}}$ was up to 2.6x higher (all $P<0.001$) (Supplementary Table 7). In agreement, dry weight (DW) greatly decreased in response to ZnO, up to 61% in roots and 83% in shoots (both $P<0.001$). The $\text{DW}_{\text{root}}/\text{DW}_{\text{shoot}}$ ratio increased up to 2.1x ($P<0.001$). Plant height decreased up to 49% in response to ZnO ($P<0.001$). Root length also decreased with increasing ZnO, with a 61% reduction at 1000 mg l^{-1} ($P<0.001$) (Supplementary Table 7). Mean root length was lowest in NP50 plants ($P=0.005$). The rest of the growth parameters measured did not show any significant differences between sources. The ET decreased up to 59% with ZnO ($P<0.001$). ET from plants at 1000 mg l^{-1} was $1078 \pm 41 \text{ g}$ of solution ($n = 14$), which was very similar to pots without plants (992 ± 24 , $n = 5$), evidencing a strong inhibition of plant transpiration. Significant effects on growth and ET started from 1 mg l^{-1} (DW_{shoot} , $\text{DW}_{\text{root}}/\text{DW}_{\text{shoot}}$, ET), 10 mg l^{-1} (all FW, DW_{root} , height), or 100 mg l^{-1} (root length), but the trend was often present at 0.1 mg l^{-1} . The $\delta^{13}\text{C}$ increased in shoots at $[\text{ZnO}] \geq 100 \text{ mg l}^{-1}$ ($P<0.001$)

(Supplementary Table 8). A similar trend was observed in roots but it did not attain significance.

Photosynthetic performance

The chlorophyll content of mature leaves decreased in response to all ZnO materials and was 25% lower than controls at 1000 mg l⁻¹ ($P<0.001$, Supplementary Table 9). Accordingly, photosynthetic efficiency was severely affected. A_s and ΦCO_2 decreased from 10 mg l⁻¹ and dropped by 79% and 75% respectively at 1000 mg l⁻¹ ($P<0.001$) (Fig. 4, Supplementary Table 9). The ΦPSII , qP , and ETR also decreased dramatically, up to 80% at 1000 mg l⁻¹ (all $P<0.001$). By contrast, F_v/F_m had only a minor reduction (6%) ($P=0.002$), whereas NPQ increased by 4.4x at 1000 mg l⁻¹ ($P=0.005$). The ΦCO_2 , F_v/F_m , ΦPSII , qP , and ETR were lower in plants under the Bulk treatment, followed by the NP50 treatment ($P=0.046$, 0.038, 0.002, 0.014, and 0.002, respectively, Fig. 4, Supplementary Table 9). Gas exchange was also affected by ZnO: g_s and E decreased up to 78% and 72%, respectively (both $P<0.001$), while VPD was 20% higher than controls at 1000 mg l⁻¹ ($P=0.002$). Finally, F_v'/F_m' was not affected by ZnO.

Root anatomy and ultrastructure

Initial light microscope exploration revealed extensive damage caused by ZnO to the roots: detachment of the epidermis, disorganisation and thickening of cell walls, and vacuolisation and death of root cells, which is indicative of increased aerenchyma formation (Supplementary Fig. 2). Plants treated with NW showed the most severe effects, with generalised apoptosis of the cortex cells that made further characterisation difficult. On the 100Kev TEM, the root epidermis showed significant loss of cell wall material in the Bulk, NP100, and NP50 treatments (Supplementary Fig. 3). The epidermal cells in the Bulk and NP50 treatments exhibited loss of turgor, protoplasm shrinkage, and accumulation of electron-dense granules in the vacuoles. In the cortex, cell-wall thickening, protoplasm shrinkage, and a high number of starch granules or amyloplasts were observed in all three treatments (Supplementary Fig. 4). Additionally, electron-dense precipitates accumulated in the intercellular spaces (Supplementary Fig. 5).

Microanalysis confirmed the presence of Zn in various locations: i) a few granules on the root surface in NP50 and NP100 that are morphologically consistent with NPs (Fig.5); ii) large amorphous precipitates between cell walls and plasma membrane in the cortex of NP50, NP100, and Bulk plants (in order of abundance, Fig.6-7), where most of Zn accumulated; and iii) small vacuoles containing Zn, P, and sometimes Ca in the rhizodermis and cortex of NP50 plants (Fig.6).

Nutrient content and distribution

Nitrogen content changed in response to ZnO, with a N_{shoot} increase of up to 24% ($P<0.001$, Supplementary Table 8). The $C_{\text{shoot}}/N_{\text{shoot}}$ ratio decreased progressively in response to increasing ZnO, reaching a 17% reduction at 1000 mg l⁻¹ ($P<0.001$). ZnO slightly increased C_{root} (~5% at 1000 mg l⁻¹, $P=0.023$) and decreased C_{shoot} (~3% at 100 mg l⁻¹, $P=0.013$). The $C_{\text{root}}/C_{\text{shoot}}$ ratio increased progressively with increasing [ZnO], up to 7% ($P=0.023$). In the roots, [Mn] and [Fe] greatly increased in response to ZnO, up to 79% and 99%, respectively, at 1000 mg l⁻¹ ($P=0.012$ and 0.004, Supplementary Table 9). Conversely, [K] showed a progressive decrease that reached 41% at 1000 mg l⁻¹ ZnO ($P<0.001$). Phosphorus in the roots increased in response to low ZnO, then decreased up to 25% at 1000 mg l⁻¹ ($P<0.001$). In the shoots, [P] was higher than controls at 10 mg l⁻¹ ZnO and above, with a peak 34% increase at 100 mg l⁻¹ ($P<0.001$). Besides, both [S] and [K] increased in response to 10-100 mg l⁻¹ ZnO, attaining levels 32% and 14% higher, respectively, than controls at 100 mg l⁻¹ ($P<0.001$ and $P=0.020$). Copper in shoots increased at 0.1 and 1 mg l⁻¹ ZnO, then gradually decreased across treatments, reaching a 30% reduction at 1000 mg l⁻¹ ($P<0.001$). Manganese in shoots progressively decreased in response to ZnO and was 66% lower than controls at the highest ZnO level ($P<0.001$). However, $[Mn]_{\text{shoot}}$ was lower in the NP50 and NP100 treatments compared to the other ZnO sources ($P<0.001$).

Discussion

Route of plant exposure to ZnO-ENMs

Our results show that ZnO-ENMs dissolve slowly in the chosen experimental conditions and that the majority was still solid at the end of the experiment (Fig. 2). Dissolved Zn reached only 4.3-7.2 mg l⁻¹ in 100 mg l⁻¹ ZnO-ENM treatments (Fig.1). This range closely agrees with dissolution experiments by Reed and co-workers, where 100 mg l⁻¹ ZnO-NP suspended in water for 60 days released 2.2-7.4 mg l⁻¹ into solution²⁷. Smaller NPs are known to dissolve more easily due to their larger surface area²⁸, which explains why [Zn]_{sol} was higher in the NP50 treatment than in the NP100 and bulk treatments (Fig.1). Solution pH was ~6 initially but gradually increased up to 7.5-8.2 in the presence of plants. This pH range is typical of wetland waters²⁹. In our study, the proportion of undissolved Zn and Al increased with increasing ZnO concentrations and solution pH. Accordingly, removal of Zn, Cd, Cu, Hg, Ni, and Pb from solution by ZnO-ENMs has been reported to increase with pH and increasing sorbent mass^{30,31}. The effect of pH on metal removal is explained by the increased deprotonation of the surface and attraction between negative hydroxyl sites and cations, while the effect of the sorbent mass is due to the increased number of binding sites. Aluminium is frequently added as a dopant to ZnO-NPs to enhance their electrical and optical properties³², so the Al mass balance in our system can serve as a proxy for the fate of doping elements. In our study, most of the Al ended up in the solid fraction, which increased with increasing ZnO, while the dissolved Al fraction decreased in the presence of ZnO (Supplementary Fig.1). However, [Al] was higher in plants grown at high [ZnO], especially for Al-doped NP50. This is consistent with the “Trojan horse effect” hypothesis, which states that ENMs might bind to other chemicals in solution and enhance their uptake by plants, leading to increased phytotoxicity. Aluminium is toxic to plants, with a reduction in root elongation as the main symptom³³. The increased uptake of Zn and Al could explain the stronger reduction in root length in NP50 plants as compared with other treatments (Supplementary Table 6). Additionally, the capacity of ZnO-ENMs for metal removal from solution might have affected the bioavailability of essential nutrients, as seen from the changes in nutrient content.

In all ZnO treatments, roots showed intense vesicularisation at the plasma membrane, but the vesicles did not contain either ZnO-ENMs or Zn. Instead, Zn was found mostly in amorphous

precipitates outside the plasma membrane, and in NP50 plants alone, in small vacuoles containing Zn, Ca, and P (Fig.6). Very few ZnO-ENMs were found attached to the root surface and none were detected in the cytoplasm (Fig.5). These observations indicate that ZnO-ENMs dissolve and the roots take up Zn^{2+} , which they mostly immobilise as Zn precipitates in the apoplast and Zn phosphates in small vacuoles. There is abundant evidence in the literature that plant roots sequester excess Zn as precipitates in the intercellular spaces or store Zn in vacuoles bound to phosphates, organic acids or phytochelatins³⁴⁻³⁹. Plants exposed to ZnO-ENMs also accumulate Zn in roots in the form of amorphous phosphates or phytates^{12,14,40}. In our study, Zn and P only co-occurred in the vacuoles of NP50 plants (Fig.6). The higher [Zn] achieved in the roots of NP50 plants might have activated vacuolar sequestration. Alternatively, NPs of this size might have been captured by endocytosis and then dissolved inside the vacuole and sequestered as phosphates. The endocytosis of entire 50 nm ZnO-NPs has been reported in hydroponically grown rice¹⁰. However, our results do not support this explanation because no NPs were detected inside the cells in our study.

The Zn isotope data support the predominant uptake of Zn^{2+} , followed by sequestration of excess Zn as precipitates and complexes in root cells. The main causes of Zn isotopic fractionation in plants are Zn speciation, compartmentalisation, and the activity of membrane transporters²⁰. Divalent Zn uptake by low-affinity transporters at the plasma membrane favours the light isotopes, which diffuse faster across membranes thanks to their smaller size^{20,41}. Hence, the relative accumulation of light Zn isotopes in the Bulk, NP100, and NP50 roots compared to ZnO (Fig. 3) can be explained by ZnO dissolution followed by Zn^{2+} uptake mediated by membrane transporters. However, NP50 roots were to some extent enriched in heavy isotopes compared to NP100 and bulk roots, although this tendency was not significant. This can be attributed to a greater number and size of Zn precipitates in the intercellular spaces of NP50 roots, which also contained more Zn relative to other treatments, and to the presence of Zn-rich vacuoles in the cortex (Fig.6-7). The formation of Zn precipitates and complexes in roots during the plant response to excess Zn^{2+} left an isotopically lighter pool of Zn^{2+} for transportation to the

shoot and favoured the accumulation of heavy isotopes in the root^{42–44}. Nevertheless, the $\delta^{66}\text{Zn}$ of NP50 roots remained lighter than the starting ZnO because this isotopic composition was still dominated by the initial transfer through the membrane, which favours light isotopes. NW roots were very damaged and had lost their structural coherence, which explains why these roots had an isotopic composition that equalled the ZnO of the NW. Further, the shoots became equally depleted in heavy isotopes in all treatments relative to the roots: $\Delta\text{Zn}_{\text{shoot-root}}$ was -0.64 ± 0.22 , -0.52 ± 0.25 , -0.57 ± 0.12 , and -0.71 ± 0.01 for Bulk, NP100, NP50, and NW50, respectively. The magnitude and direction of $\Delta\text{Zn}_{\text{shoot-root}}$ are in the same range as previously observed in *P. australis* in response to ZnCl_2 toxicity⁴⁴. Depletion of heavy Zn isotopes during Zn transport to the shoot is attributed to preferential sequestration of heavy isotopes in the root, the activity the membrane transporters during Zn loading into the xylem, and bulk flow^{44–46}. Conversely, there is no isotopic fractionation when Zn is transported in complexes up the shoot due to the bigger mass of the complexes⁴⁷. The same likely applies to ZnO-ENMs. Hence, our isotope data indicate that Zn was predominantly transported up the shoot as Zn^{2+} , regardless of the ZnO source, and that plants roots are an effective barrier against ZnO-ENM transport up the shoot, which is in agreement with our TEM observations. If ZnO-ENM had been transported through the plant without dissolution, then no isotopic fractionation would have been detected during Zn uptake and transport in the plants. ZnO-NPs in the apoplast reportedly can reach the symplast by endocytosis¹¹ or through the discontinuity of Casparian bands^{6,14}. However, ZnO-NPs in our study were found on the surface of the root but not in the apoplast, indicating that the rhizodermis was an effective barrier. Similarly, recent research shows that ZnO-NPs are unlikely to reach the shoots unless roots are damaged¹³. Finally, the fractionation of Zn isotopes in control plants is consistent with the plants' response to Zn-deficiency, which results in Zn uptake and transport to the shoots in the form of Zn complexes, with root exudates enriched in heavy isotopes⁴⁸. The $\delta^{66}\text{Zn}$ of all the ZnO materials was remarkably similar (0.33‰) and the value was consistent with reported ranges for both ZnO-ENMs (-0.31 to 0.28%)⁴⁹ and natural Zn minerals like hydrozincite (0 – 0.30%)⁵⁰.

Phytotoxicity

Chronic exposure to high levels of ZnO-ENMs decreased growth, chlorophyll content, and photosynthetic assimilation in *P. australis* (Fig.4, Supplementary Tables 6-7). Biomass allocation, nutrient uptake and distribution, and fractionation of C isotopes were also altered by ZnO-ENMs (Supplementary Tables 8-9). Similar effects have been previously described in aquatic macrophytes treated with toxic levels of ZnO-ENMs^{4-6,8,10,51,52}, Zn²⁺ (reviewed by²⁰), and other metals⁵³⁻⁵⁶. In our previous research on *P. australis*, exposure to 2 mM ZnCl₂ (131 mg l⁻¹ Zn in solution) for 40 days caused a height reduction of 25%⁴⁴. Song and coworkers⁴ reported a ~50% reduction in height after exposure to 100 mg l⁻¹ ZnO NP50 (only 4.5 mg l⁻¹ Zn in solution) for 35 days⁴. Even though [Zn²⁺] was lower in the latter study, the effects were more severe and attributed to direct root contact with ZnO-NPs. Accordingly, we report a height decrease of 43% after three months at 100 mg l⁻¹ ZnO (3.5-7.2 mg l⁻¹ in solution), irrespective of particle size. The magnitude of the effect paralleled the Song *et al.* study despite the longer exposure time and larger particle sizes of the Bulk, NP100, and NW treatments. To sum up, ZnO is more toxic to *P. australis* than ZnCl₂. The total ZnO added to the system is the most important factor to explain the impact of ZnO-ENMs on plant growth, rather than [Zn²⁺] in solution and particle size. The toxicity cannot be attributed to the osmotic effect of the increased [Zn²⁺]. The conductance (EC) did not increase with increasing ZnO, which remained mostly undissolved. This clearly demonstrates that undissolved ZnO plays a key role in ENM phytotoxicity. To correctly assess the environmental risks of ZnO-ENMs, field studies should include the solid ZnO fraction in sediments, rather than just focus on ZnO-ENM levels in the water. However, particle size was relevant for ZnO-ENM impacts on root growth and [Mn]_{shoot} due to the greater dissolution of smaller NPs.

The lower photosynthetic rates can be explained by stomatal closure and root malfunction leading to water deficit, higher $\delta^{13}\text{C}$, lower chlorophyll content, and nutritional imbalance. Of particular interest were the changes in Mn content, which greatly decreased in shoots in a dose-dependent response to [ZnO] and particle size (Supplementary Table 9). It is unlikely that this

decrease in $[Mn]_{shoot}$ is caused by Mn removal from solution by ENMs. The removal efficiency is low for Mn⁵⁷ and the $[Mn]_{root}$ was high, proving that Mn uptake was not impaired. We propose that excess Zn²⁺ might inhibit or compete for Mn²⁺ transporters involved in Mn root-to-shoot transport, like AtZIP1 and ATZIP2. These carriers transport Zn and Mn, are expressed in the root vasculature, and mediate Mn radial movement towards the xylem and xylem loading⁵⁸. Manganese has a key role as a catalyst of the oxygen-evolving complex of PSII and its deficiency greatly reduces photosynthesis⁵⁹. Gas exchange and chlorophyll fluorescence data taken at the same time confirm lower electron transport efficiency. E and g_s decreased, indicating that the stomatal opening was strongly inhibited. The reduced gas exchange could lower A_s by restricting CO₂ availability. The parallel increase in $\delta^{13}C$ of shoot and root dry matter also supports this conclusion. However, C_i was not affected in our study. Helophytes take up CO₂ dissolved in water by the roots, and it diffuses towards the photosynthetic tissues via the aerenchyma⁶⁰. This alternative source of CO₂ can contribute significantly to C_i^{61,62}. The small 5% reduction in F_v/F_m in dark-adapted leaves and the unaltered F_v'/F_m' showed that PSII was mostly functional. By contrast, the $\Phi PSII$, qP, ΦCO_2 , and ETR were severely reduced in light-adapted leaves, while qN and NPQ increased. Hence, we attribute the reduced ΦCO_2 and A_s to decreased stomatal conductance and lower efficiency of electron transport downstream due to an Mn deficiency that caused PSII to become easily saturated by light. Reduced chlorophyll content, A_s, g_{ss}, E, C_i, F_v/F_m, qP, and ETR coupled with increased NPQ have been reported in terrestrial plants exposed to toxic levels of ZnO-ENMs^{63,64}. In agreement, the aquatic plants *Azolla filiculoides* and *Lemna minor* have shown severely reduced growth, chlorophyll content and F_v/F_m after exposure to ZnO-ENMs at pH 4.5-5.5^{5,10,65}. Remarkably, growth and F_v/F_m in *L. minor* were not equally reduced at pH 8, due to the lower NP dissolution⁶⁵. In our study, *P. australis* progressively basified the growth media, which reached pH~8 at the end of the experiment. This high final pH could explain the limited effect of ZnO on F_v/F_m. The $\delta^{13}C_{shoot}$ was within -26.7 to -30.7 ‰, which is in agreement with values previously reported for C3 helophytes^{53,66}. In C3 plants, diffusion of atmospheric CO₂ through the stomatal pore and C fixation by RuBisCO favour ¹²C⁶⁷. During stomatal closure, RuBisCO continues consuming

intercellular CO₂ and the $\delta^{13}\text{C}_{\text{shoot}}$ increases as ^{12}C is depleted⁶⁸. In our study, $\delta^{13}\text{C}_{\text{shoot}}$ and $\delta^{13}\text{C}_{\text{root}}$ increased (~1‰) in response to high ZnO. This, in the context of reduced transpiration, is generally caused by Ci exhaustion⁶⁷. However, our gas exchange data do not indicate Ci depletion. While *P. australis* mainly assimilates atmospheric C, it can also take up CO₂ dissolved in water by the roots⁶⁰. Plants that assimilate more CO₂ by this route show higher $\delta^{13}\text{C}$, as seen when comparing submerged aquatic plants relative to helophytes⁶⁶. The assimilation of a larger proportion of CO₂ from the roots during stomatal closure can explain a higher $\delta^{13}\text{C}$ while maintaining Ci levels. In agreement, we observed increased root aerenchyma development in response to excess Zn. We found no previous record of $\delta^{13}\text{C}$ in plants exposed to toxic levels of ZnO-ENMs, although *Iris pseudacorus* grown in 200 mg l⁻¹ ZnCl₂ showed a similar increase of $\delta^{13}\text{C}_{\text{shoot}}$ ⁵³. Our experiment shows that ZnO-ENMs are toxic from 1 mg l⁻¹. Effects at this concentration include reduced growth, allocation of new biomass to the roots and rhizomes instead of the photosynthetic tissues, and restriction of transpiration. These levels are high compared to the few existing records of ZnO-ENMs in surface waters: there are up to 1.84 µg l⁻¹ ZnO NMs in the surface waters of Singapore⁶⁹ and just 5 ng l⁻¹ in Canada⁷⁰. However, recent modelling studies estimate ZnO-ENM concentrations of 10⁻⁶ to 1 µg l⁻¹ in surface waters and 11-32 mg kg⁻¹ in sediments⁷¹⁻⁷³. Current levels predicted for the sediments would cause substantial toxic effects on *P. australis*. Besides, the said models have important limitations, and the real concentrations are likely to be locally higher and to increase in coming years⁷⁴.

Conclusion

Emerging nano-pollutants like ZnO-ENM are increasingly discharged into surface waters and they accumulate in sediments. This is a cause of major concern because of our limited understanding of the mechanisms of ZnO-ENM uptake and toxicity in wetland plants, which play key ecological roles in aquatic ecosystems. Besides, there is an ongoing controversy about the capacity of ENMs to enter plant roots and be transported to the shoots. Our research

concludes that ZnO-ENM dissolve before uptake by plant roots and that they are not transported to the shoots. Nanoparticles smaller than 50 nm dissolve faster than the larger particles and are more toxic to plants. Exposure to ZnO-ENM takes place mostly through the uptake of dissolved Zn^{2+} , but also through direct contact with the root surface. The mechanisms of action of ZnO-ENM adsorbed onto the root surface require further investigation. In *Phragmites australis*, ZnO-ENM reduce shoot and root growth, transpiration, and photosynthetic rate, while inducing changes in nutrient uptake and distribution. This could be detrimental to the environmental health of aquatic ecosystems and their capacity to sequester carbon. Wetlands are one of the major carbon sinks globally. Pollutants that compromise the biomass production of wetland plants can increase global carbon emissions, of vital importance in the current context of climate change. In conclusion, current and future ZnO-ENM levels in sediments could pose a significant risk for aquatic plants and ecosystems. Our research also evidences the importance of considering the undissolved fraction, exposure time, and NP size to correctly evaluate the environmental risk of nanomaterials.

Acknowledgements

This project has received funding from the European Union's Horizon 2020 research and innovation programme under the Marie Skłodowska-Curie grant agreement NANOREM No 704957. Franck Poitrasson is funded by the French Centre National de la Recherche Scientifique. We are grateful for the technical assistance of Joan Martorell and Luís López with TEM microanalysis; Manuel Henry and Jérôme Chmeleff with Zn isotope analysis; and Josep Mata, Marta Pintó, and Xavier García with greenhouse tasks and photosynthesis measurements. We thank Sheela Paramjothy for her help with maintaining the experiment.

- 587 1 A. A. Keller, S. McFerran, A. Lazareva and S. Suh, Global life cycle releases of engineered
588 nanomaterials, *Journal of Nanoparticle Research*, DOI:10.1007/s11051-013-1692-4.
- 589 2 T. Y. Sun, F. Gottschalk, K. Hungerbühler and B. Nowack, Comprehensive probabilistic
590 modelling of environmental emissions of engineered nanomaterials, *Environmental*
591 *Pollution*, 2014, **185**, 69–76.
- 592 3 J. M. Caffrey, C. Monahan and D. Tierney, Factors influencing the distribution of aquatic
593 plant communities in Irish canals, *Hydrobiologia*, 2006, **570**, 133–139.
- 594 4 U. Song and S. Lee, Phytotoxicity and accumulation of zinc oxide nanoparticles on the
595 aquatic plants *Hydrilla verticillata* and *Phragmites Australis*: leaf-type-dependent responses,
596 *Environmental Science and Pollution Research*, 2016, **23**, 8539–8545.
- 597 5 G. S. Zarate-Cruz, H. A. Zavaleta-Mancera, A. Alarcón and L. F. Jiménez-García, Phytotoxicity
598 of ZnO nanoparticles on the aquatic fern *Azolla filiculoides* Lam, *Agrociencia*, 2016, **50**, 677–
599 691.
- 600 6 D. Zhang, T. Hua, F. Xiao, C. Chen, R. M. Gersberg, Y. Liu, D. Stuckey, W. J. Ng and S. K. Tan,
601 Phytotoxicity and bioaccumulation of ZnO nanoparticles in *Schoenoplectus*
602 *tabernaemontani*, *Chemosphere*, 2015, **120**, 211–219.
- 603 7 C. Hu, X. Liu, X. Li and Y. Zhao, Evaluation of growth and biochemical indicators of *Salvinia*
604 *natans* exposed to zinc oxide nanoparticles and zinc accumulation in plants., *Environmental*
605 *science and pollution research international*, 2014, **21**, 732–9.
- 606 8 C. Hu, Y. Liu, X. Li and M. Li, Biochemical responses of duckweed (*Spirodela polyrhiza*) to
607 zinc oxide nanoparticles, *Archives of Environmental Contamination and Toxicology*, 2013,
608 **64**, 643–651.
- 609 9 M. Thwala, N. Musee, L. Sikhwivhilu and V. Wepener, The oxidative toxicity of Ag and ZnO
610 nanoparticles towards the aquatic plant *Spirodela punctata* and the role of testing media
611 parameters, *Environmental Science: Processes & Impacts*, 2013, **15**, 1830.
- 612 10 X. Chen, J. O'Halloran and M. A. K. Jansen, Time Matters: the Toxicity of Zinc Oxide
613 Nanoparticles to *Lemna minor* L. Increases with Exposure Time, *Water, Air, & Soil Pollution*,
614 2018, **229**, 99.
- 615 11 J. Chen, R. Dou, Z. Yang, T. You, X. Gao and L. Wang, Phytotoxicity and bioaccumulation of
616 zinc oxide nanoparticles in rice (*Oryza sativa* L.), *Plant Physiology and Biochemistry*, 2018,
617 **130**, 604–612.
- 618 12 P. Wang, N. W. Menzies, E. Lombi, B. A. McKenna, B. Johannessen, C. J. Glover, P. Kappen
619 and P. M. Kopittke, Fate of ZnO Nanoparticles in Soils and Cowpea (*Vigna unguiculata*),
620 *Environmental Science & Technology*, 2013, **47**, 13822–13830.
- 621 13 T. N. M. da Cruz, S. M. Savassa, M. H. F. Gomes, E. S. Rodrigues, N. M. Duran, E. de Almeida,
622 A. P. Martinelli and H. W. P. de Carvalho, Shedding light on the mechanisms of absorption
623 and transport of ZnO nanoparticles by plants *via in vivo* X-ray spectroscopy, *Environmental*
624 *Science: Nano*, 2017, **4**, 2367–2376.
- 625 14 J. Lv, S. Zhang, L. Luo, J. Zhang, K. Yang and P. Christie, Accumulation, speciation and uptake
626 pathway of ZnO nanoparticles in maize, *Environmental Science: Nano*, 2015, **2**, 68–77.
- 627 15 D. Lin and B. Xing, Root Uptake and Phytotoxicity of ZnO Nanoparticles, *Environmental*
628 *Science & Technology*, 2008, **42**, 5580–5585.
- 629 16 J. A. Hernandez-Viezcás, H. Castillo-Michel, J. C. Andrews, M. Cotte, C. Rico, J. R. Peralta-
630 Videá, Y. Ge, J. H. Priester, P. A. Holden and J. L. Gardea-Torresdey, In Situ Synchrotron X-
631 ray Fluorescence Mapping and Speciation of CeO₂ and ZnO Nanoparticles in Soil Cultivated
632 Soybean (*Glycine max*), *ACS Nano*, 2013, **7**, 1415–1423.
- 633 17 A. R. English and G. K. Voeltz, Interconnections with Other Organelles, *Cold Spring Harbor*
634 *perspectives in biology*, 2013, 1–16.

- 18 C. Caldelas, S. Dong, J. L. Araus and D. Jakob Weiss, Zinc isotopic fractionation in *Phragmites australis* in response to toxic levels of zinc, *Journal of Experimental Botany*, DOI:10.1093/jxb/erq414.
- 19 A. M. Aucour, S. Pichat, M. R. MacNair and P. Oger, Fractionation of stable zinc isotopes in the zinc hyperaccumulator *Arabidopsis halleri* and nonaccumulator *arabidopsis petraea*, *Environmental Science and Technology*, 2011, **45**, 9212–9217.
- 20 C. Caldelas and D. J. Weiss, Zinc Homeostasis and isotopic fractionation in plants: a review, *Plant and Soil*, 2017, **411**, 17–46.
- 21 Emanuel. Epstein, *Mineral nutrition of plants: principles and perspectives.*, Wiley, 1972.
- 22 K. Peel, D. Weiss, J. Chapman, T. Arnold and B. Coles, A simple combined sample–standard bracketing and inter-element correction procedure for accurate mass bias correction and precise Zn and Cu isotope ratio measurements, *J. Anal. At. Spectrom.*, 2008, **23**, 103–110.
- 23 C. Archer, M. B. Andersen, C. Cloquet, T. M. Conway, S. Dong, M. Ellwood, R. Moore, J. Nelson, M. Rehkämper, O. Rouxel, M. Samanta, K.-C. C. Shin, Y. Sohrin, S. Takano and L. Wasylenki, Inter-calibration of a proposed new primary reference standard AA-ETH Zn for zinc isotopic analysis, *Journal of Analytical Atomic Spectrometry*, 2017, **32**, 415–419.
- 24 E. Smolders, L. Versieren, D. Shuofei, N. Mattielli, D. Weiss, I. Petrov and F. Degryse, Isotopic fractionation of Zn in tomato plants suggests the role of root exudates on Zn uptake, *Plant and Soil*, 2013, **370**, 605–613.
- 25 B. Krugh, L. Bickham and D. Miles, The solid-state chlorophyll meter: a novel instrument for rapidly and accurately determining the chlorophyll concentrations in seedling leaves, *Maize Genetics Cooperation Newsletter*, 1994, **68**, 25–27.
- 26 B. Genty, J.-M. Briantais and N. R. Baker, The relationship between the quantum yield of photosynthetic electron transport and quenching of chlorophyll fluorescence, *Biochimica et Biophysica Acta (BBA) - General Subjects*, 1989, **990**, 87–92.
- 27 R. B. Reed, D. A. Ladner, C. P. Higgins, P. Westerhoff and J. F. Ranville, Solubility of nano-zinc oxide in environmentally and biologically important matrices., *Environmental toxicology and chemistry*, 2012, **31**, 93–9.
- 28 I. A. Mudunkotuwa, T. Rupasinghe, C.-M. Wu and V. H. Grassian, Dissolution of ZnO Nanoparticles at Circumneutral pH: A Study of Size Effects in the Presence and Absence of Citric Acid, *Langmuir*, 2012, **28**, 396–403.
- 29 P. J. Gerla, Can pH and electrical conductivity monitoring reveal spatial and temporal patterns in wetland geochemical processes?, *Hydrology and Earth System Sciences Discussions*, 2013, **10**, 699–728.
- 30 S. Mahdavi, M. Jalali and A. Afkhami, Removal of heavy metals from aqueous solutions using Fe₃O₄, ZnO, and CuO nanoparticles, *Journal of Nanoparticle Research*, 2012, **14**, 846.
- 31 T. Sheela, Y. A. Nayaka, R. Viswanatha, S. Basavanna and T. G. Venkatesha, Kinetics and thermodynamics studies on the adsorption of Zn(II), Cd(II) and Hg(II) from aqueous solution using zinc oxide nanoparticles, *Powder Technology*, 2012, **217**, 163–170.
- 32 P. Zhang, R. Y. Hong, Q. Chen, W. G. Feng and D. Badami, Aluminum-doped zinc oxide powders: synthesis, properties and application, *Journal of Materials Science: Materials in Electronics*, 2014, **25**, 678–692.
- 33 S. R. Imadi, S. Waseem, A. G. Kazi, M. M. Azooz and P. Ahmad, in *Plant Metal Interaction*, Elsevier, 2016, pp. 1–20.
- 34 A. Straczek, G. Sarret, A. Manceau, P. Hinsinger, N. Geoffroy and B. Jaillard, Zinc distribution and speciation in roots of various genotypes of tobacco exposed to Zn, *Environmental and Experimental Botany*, 2008, **63**, 80–90.
- 35 W.-Y. Song, D. G. Mendoza-Cózatl, Y. Lee, J. I. Schroeder, S.-N. Ahn, H.-S. Lee, T. Wicker and E. Martinoia, Phytochelatin-metal(loid) transport into vacuoles shows different substrate preferences in barley and *Arabidopsis*., *Plant, cell & environment*, 2014, **37**, 1192–201.

- 36 A. C. Monsanto, P. Kappen, Y. Wang, P. J. Pigram, A. J. M. Baker and C. Tang, In vivo speciation of zinc in *Noccaea caerulescens* in response to nitrogen form and zinc exposure, *Plant and Soil*, 2011, **348**, 167–183.
- 37 G. Sarret, P. Saumitou-Laprade, V. Bert, O. Proux, J.-L. Hazemann, A. Traverse, M. a Marcus and A. Manceau, Forms of zinc accumulated in the hyperaccumulator *Arabidopsis halleri*., *Plant physiology*, 2002, **130**, 1815–26.
- 38 R. F. M. Van Steveninck, M. E. Van Steveninck, D. R. Fernando, W. J. Horst and H. Marschner, Deposition of Zinc Phytate in Globular Bodies in Roots of *Deschampsia caespitosa* Ecotypes; a Detoxification Mechanism?, *Journal of Plant Physiology*, 1987, **131**, 247–257.
- 39 D. Neumann and U. zur Nieden, Silicon and heavy metal tolerance of higher plants, *Phytochemistry*, 2001, **56**, 685–692.
- 40 S. Moghaddasi, A. Fotovat, F. Karimzadeh, H. R. Khazaei, R. Khorassani and A. Lakzian, Effects of coated and non-coated ZnO nanoparticles on cucumber seedlings grown in gel chamber, *Archives of Agronomy and Soil Science*, 2017, **63**, 1108–1120.
- 41 S. G. John, R. W. Geis, M. a. Saito and E. a. Boyle, Zinc isotope fractionation during high-affinity and low-affinity zinc transport by the marine diatom *Thalassiosira oceanica*, *Limnology and Oceanography*, 2007, **52**, 2710–2714.
- 42 T. Fujii and F. Albarède, Ab initio calculation of the Zn isotope effect in phosphates, citrates, and malates and applications to plants and soil, *PLoS ONE*, 2012, **7**, e30726.
- 43 T. Markovic, S. Manzoor, E. Humphreys-Williams, G. Kirk, R. Vilar and D. J. Weiss, Experimental determination of zinc isotope fractionation in complexes with the phytosiderophore 2'-deoxymugeneic acid (DMA) and its structural analogues, and implications for plant uptake mechanisms, *Environmental Science & Technology*, 2016, [acs.est.6b00566](https://doi.org/10.1021/acs.est.6b00566).
- 44 C. Caldelas, S. Dong, J. L. Araus and D. J. Weiss, Zinc isotopic fractionation in *Phragmites australis* in response to toxic levels of zinc, *Journal of Experimental Botany*, 2011, **62**, 2169–2178.
- 45 J. Viers, P. Oliva, A. Nonell, A. Gélabert, J. E. Sonke, R. Freydier, R. Gainville and B. Dupré, Evidence of Zn isotopic fractionation in a soil-plant system of a pristine tropical watershed (Nsimi, Cameroon), *Chemical Geology*, 2007, **239**, 124–137.
- 46 E. Couder, N. Mattielli, T. Drouet, E. Smolders, B. Delvaux, A. Iserentant, C. Meeus, C. Maerschalk, S. Opfergelt and D. Houben, Transpiration flow controls Zn transport in *Brassica napus* and *Lolium multiflorum* under toxic levels as evidenced from isotopic fractionation, *Comptes Rendus Geoscience*, DOI:10.1016/j.crte.2015.05.004.
- 47 D. J. Weiss, T. F. D. Mason, F. J. Zhao, G. J. D. Kirk, B. J. Coles and M. S. a Horstwood, Isotopic discrimination of zinc in higher plants, *New Phytologist*, 2005, **165**, 703–710.
- 48 T. Arnold, G. J. D. Kirk, M. Wissuwa, M. Frei, F. J. Zhao, T. F. D. Mason and D. J. Weiss, Evidence for the mechanisms of zinc uptake by rice using isotope fractionation, *Plant Cell and Environment*, 2010, **33**, 370–381.
- 49 F. Lerner and M. Rehkämper, Evaluation of stable isotope tracing for ZnO nanomaterials—new constraints from high precision isotope analyses and modelling, *Environmental Science and Technology*, 2012, **46**, 4149–4158.
- 50 N. Mondillo, J. J. Wilkinson, M. Boni, D. J. Weiss and R. Mathur, A global assessment of Zn isotope fractionation in secondary Zn minerals from sulfide and non-sulfide ore deposits and model for fractionation control, *Chemical Geology*, 2018, **500**, 182–193.
- 51 D. Haisel, T. Cyrusová, T. Vaněk and R. Podlipná, The effect of nanoparticles on the photosynthetic pigments in cadmium—zinc interactions, *Environmental Science and Pollution Research*, 2019, **26**, 4147–4151.
- 52 M. Asztemborska, M. Bembenek, M. Jakubiak, R. Stęborowski and G. Bystrzejewska-Piotrowska, The Effect of Nanoparticles with Sorption Capacity on the Bioaccumulation of

- Divalent Ions by Aquatic Plants, *International Journal of Environmental Research*, 2018, **12**, 245–253.
- 53 C. Caldelas, J. L. L. Araus, A. Febrero and J. Bort, Accumulation and toxic effects of chromium and zinc in *Iris pseudacorus* L, *Acta Physiologiae Plantarum*, 2012, **34**, 1217–1228.
- 54 C. Caldelas, S. Iglesia-turiño, J. L. Araus, J. Bort and A. Febrero, Physiological responses of *Eichhornia crassipes* [Mart .] Solms to the combined exposure to excess nutrients and Hg ., 2009, **21**, 1–12.
- 55 A. Basile, S. Sorbo, B. Conte, R. C. Cobiainchi, F. Trinchella, C. Capasso and V. Carginale, Toxicity, Accumulation, and Removal of Heavy Metals by Three Aquatic Macrophytes, *International Journal of Phytoremediation*, 2012, **14**, 374–387.
- 56 M. B. Costa, F. V. Tavares, C. B. Martinez, I. G. Colares and C. de M. G. Martins, Accumulation and effects of copper on aquatic macrophytes *Potamogeton pectinatus* L.: Potential application to environmental monitoring and phytoremediation, *Ecotoxicology and Environmental Safety*, 2018, **155**, 117–124.
- 57 A. T. Le, S.-Y. Pung, S. Sreekantan, A. Matsuda and D. P. Huynh, Mechanisms of removal of heavy metal ions by ZnO particles, *Heliyon*, 2019, **5**, e01440.
- 58 M. J. Milner, J. Seamon, E. Craft and L. V. Kochian, Transport properties of members of the ZIP family in plants and their role in Zn and Mn homeostasis., *Journal of experimental botany*, 2013, **64**, 369–81.
- 59 S. B. Schmidt, P. E. Jensen and S. Husted, Manganese Deficiency in Plants: The Impact on Photosystem II, *Trends in Plant Science*, 2016, **21**, 622–632.
- 60 H. Brix, Uptake and photosynthetic utilization of sediment-derived carbon by *Phragmites australis* (Cav.) Trin. ex Steudel, *Aquatic Botany*, 1990, **38**, 377–389.
- 61 J. V. H. Constable, J. B. Grace and D. J. Longstreth, High Carbon Dioxide Concentrations in Aerenchyma of *Typha latifolia*, *American Journal of Botany*, 1992, **79**, 415.
- 62 Wium-Andersen, Photosynthetic Uptake of Free CO₂, by the Roots of *Lobelia dortmanna*, *Physiologia Plantarum*, 1971, **25**, 245–248.
- 63 X. P. Wang, Q. Q. Li, Z. M. Pei and S. C. Wang, Effects of zinc oxide nanoparticles on the growth, photosynthetic traits, and antioxidative enzymes in tomato plants, *Biologia Plantarum*, 2018, **62**, 801–808.
- 64 D. K. Tripathi, R. K. Mishra, S. S. Singh, S. S. Singh, K. Vishwakarma, S. Sharma, V. P. Singh, P. K. Singh, S. M. Prasad, N. K. Dubey, A. C. Pandey, S. Sahi and D. K. Chauhan, Nitric Oxide Ameliorates Zinc Oxide Nanoparticles Phytotoxicity in Wheat Seedlings: Implication of the Ascorbate–Glutathione Cycle, *Frontiers in Plant Science*, 2017, **8**, 1.
- 65 X. Chen, J. O'Halloran and M. A. K. Jansen, The toxicity of zinc oxide nanoparticles to *Lemna minor* (L.) is predominantly caused by dissolved Zn, *Aquatic Toxicology*, 2016, **174**, 46–53.
- 66 E. Chappuis, V. Serriñá, E. Martí, E. Ballesteros and E. Gacia, Decrypting stable-isotope ($\delta^{13}\text{C}$ and $\delta^{15}\text{N}$) variability in aquatic plants, *Freshwater Biology*, DOI:10.1111/fwb.12996.
- 67 G. D. Farquhar, J. R. Ehleringer and K. T. Hubick, Carbon Isotope Discrimination and Photosynthesis, *Annual Review of Plant Physiology and Plant Molecular Biology*, 1989, **40**, 503–537.
- 68 G. Farquhar, M. O'Leary and J. Berry, On the Relationship Between Carbon Isotope Discrimination and the Intercellular Carbon Dioxide Concentration in Leaves, *Australian Journal of Plant Physiology*, 1982, **9**, 121.
- 69 S. M. Majedi, H. K. Lee and B. C. Kelly, Chemometric Analytical Approach for the Cloud Point Extraction and Inductively Coupled Plasma Mass Spectrometric Determination of Zinc Oxide Nanoparticles in Water Samples, *Analytical Chemistry*, 2012, **84**, 6546–6552.
- 70 M. Hadioui, V. Merdzan and K. J. Wilkinson, Detection and Characterization of ZnO Nanoparticles in Surface and Waste Waters Using Single Particle ICPMS, *Environmental Science & Technology*, 2015, **49**, 6141–6148.

- 71 T. Y. Sun, N. A. Bornhöft, K. Hungerbühler and B. Nowack, Dynamic Probabilistic Modeling of Environmental Emissions of Engineered Nanomaterials, *Environmental Science & Technology*, 2016, **50**, 4701–4711.
- 72 K. L. Garner, S. Suh and A. A. Keller, Assessing the Risk of Engineered Nanomaterials in the Environment: Development and Application of the nanoFate Model, *Environmental Science & Technology*, 2017, **51**, 5541–5551.
- 73 E. Dumont, A. C. Johnson, V. D. J. Keller and R. J. Williams, Nano silver and nano zinc-oxide in surface waters - exposure estimation for Europe at high spatial and temporal resolution., *Environmental pollution (Barking, Essex : 1987)*, 2015, **196**, 341–9.
- 74 J. R. Lead, G. E. Batley, P. J. J. Alvarez, M.-N. Croteau, R. D. Handy, M. J. McLaughlin, J. D. Judy and K. Schirmer, Nanomaterials in the environment: Behavior, fate, bioavailability, and effects-An updated review, *Environmental Toxicology and Chemistry*, 2018, **37**, 2029–2063.
- 75 W. Bussler, Epstein, E.: Mineral Nutrition of Plants: Principles and Perspectives. John Wiley and Sons, Inc., New York, London, Sydney, Toronto. 1972. 412 Seiten, 23 × 16 cm, zahlreiche Abbildungen, £ 4.85, *Zeitschrift für Pflanzenernährung und Bodenkunde*, 1972, **132**, 158–159.

Figures

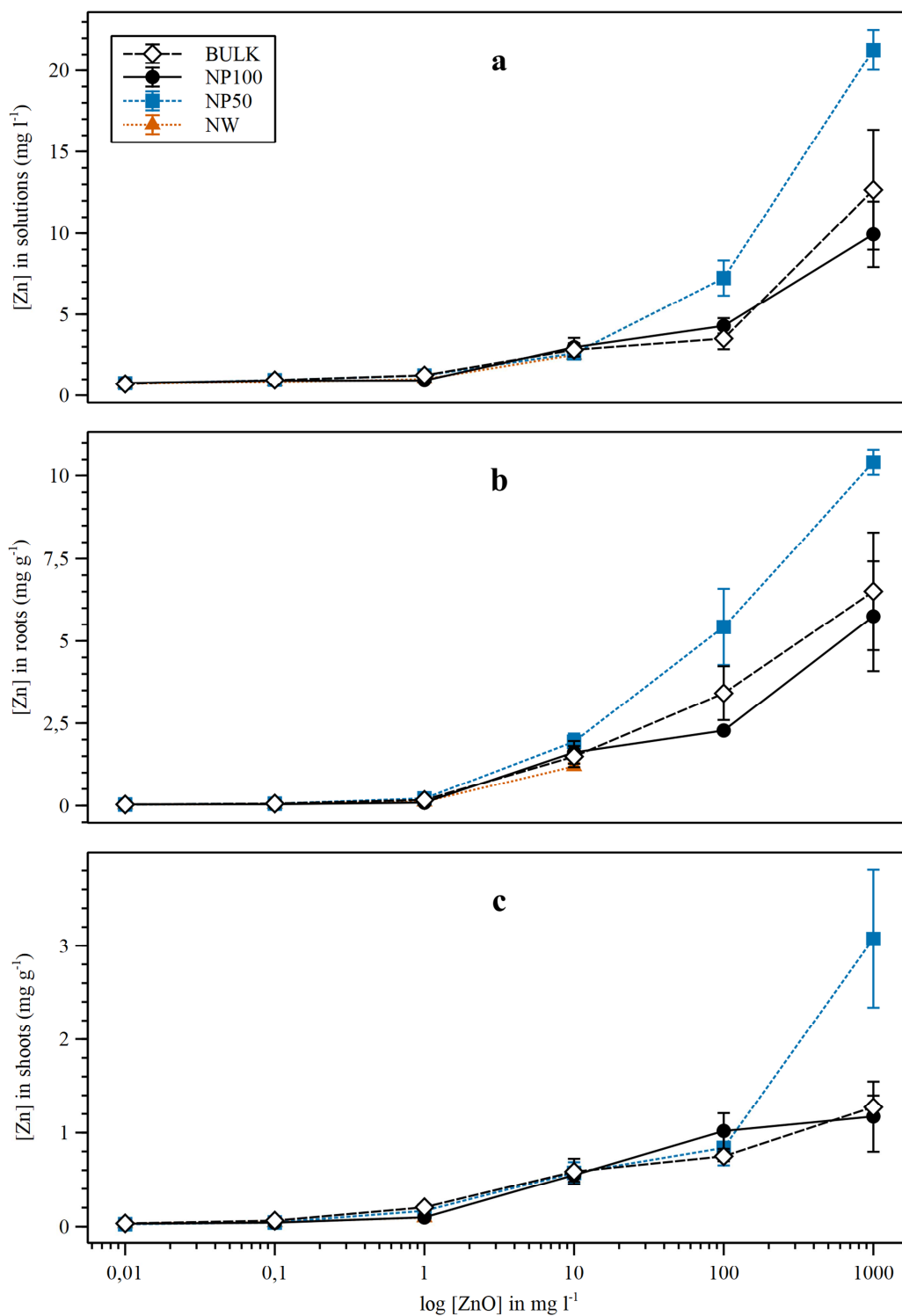


Fig. 1. Zinc concentration in nutrient solutions (top), roots (middle), and shoots (bottom). Plants were exposed to four different ZnO sources: micron-size (Bulk), NP < 100 nm (NP100), NP < 50 nm (NP50), and nanowires of 50 nm diameter (NW). Controls (0 mg l⁻¹ ZnO) are represented

as 0.01 mg l⁻¹. Data represent means ±SE, where n = 4. Concentration data are expressed in mg l⁻¹ for the growth solutions and in mg g⁻¹ for plant samples.

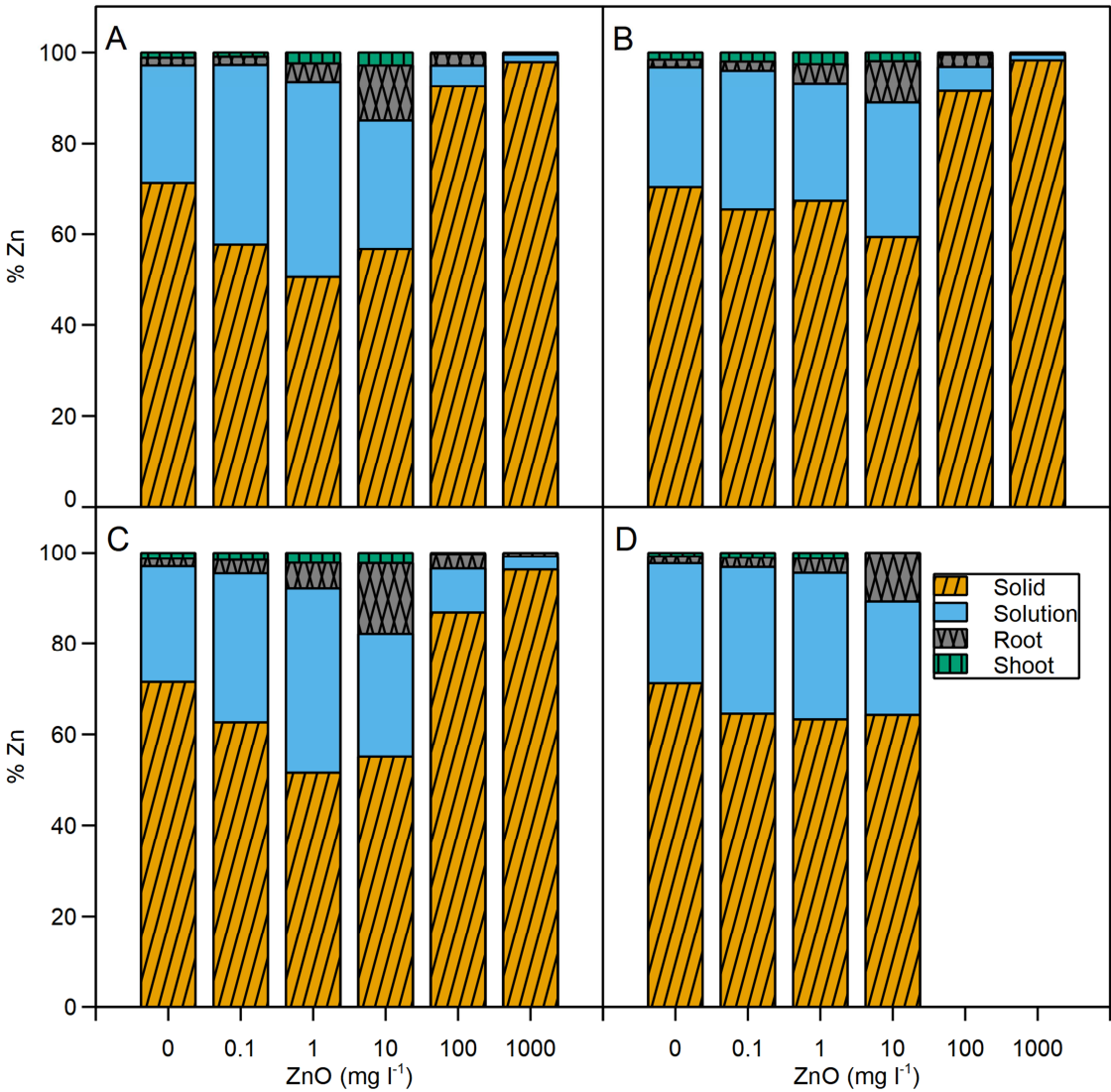


Fig. 2. Distribution of Al across the different pools. Plants were treated with four different ZnO sources: micron-size (Bulk), NP < 100 nm (NP100), NP < 50 nm (NP50), and nanowires of 50 nm diameter (NW). Data represent means, where n = 4, expressed as Al % relative to the total Al incorporated into the system from the nutrient solution and ZnO treatments.

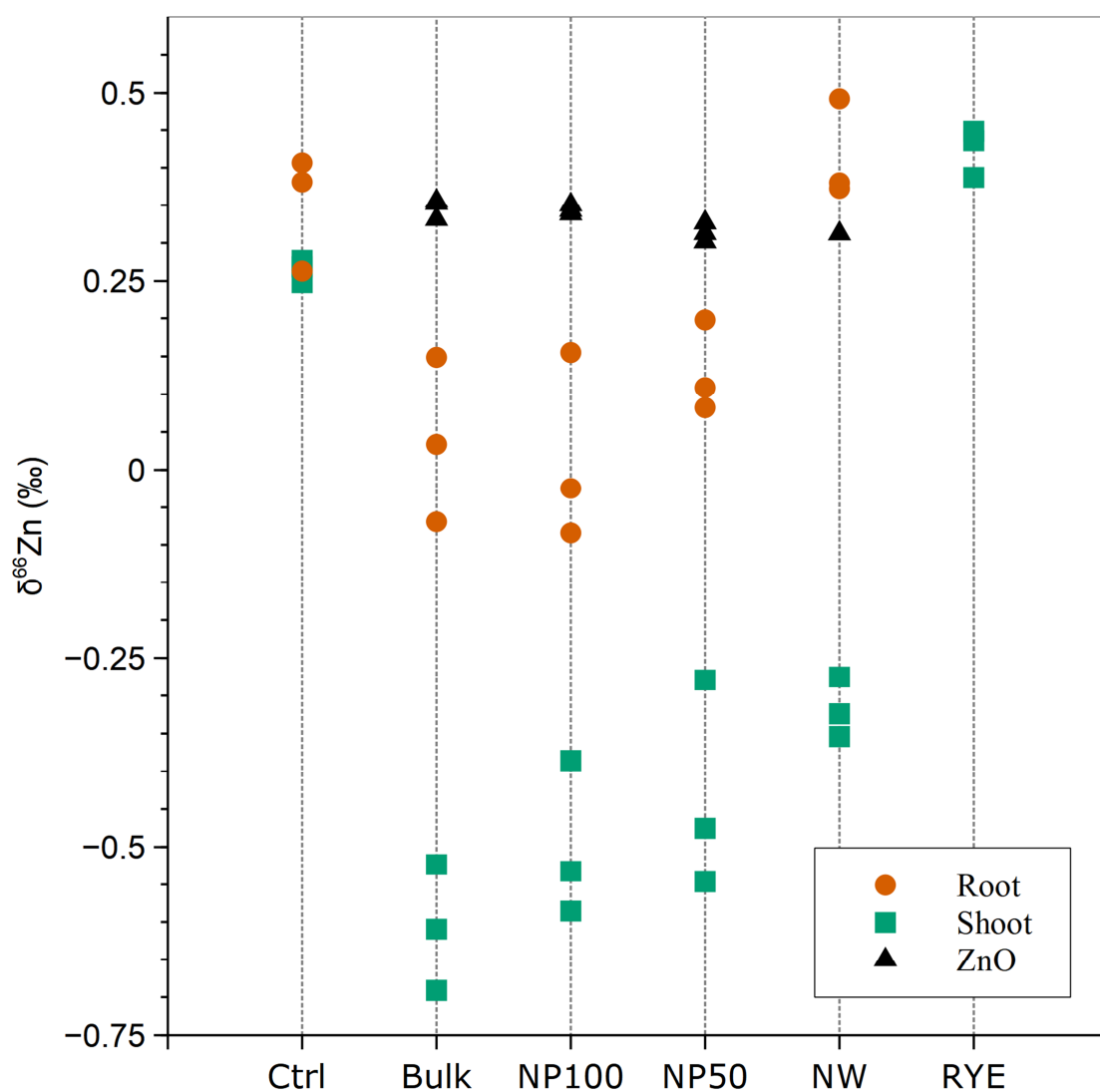


Fig. 3. Zinc isotopic composition of ZnO materials, plants, and the BCR-281 (RYE) reference material. Plants were treated with four different ZnO sources at 100 mg l^{-1} : micron-size (Bulk), NP < 100 nm (NP100), NP < 50 nm (NP50), and nanowires of 50 nm diameter (NW). Data are expressed relative to JMC Zn.

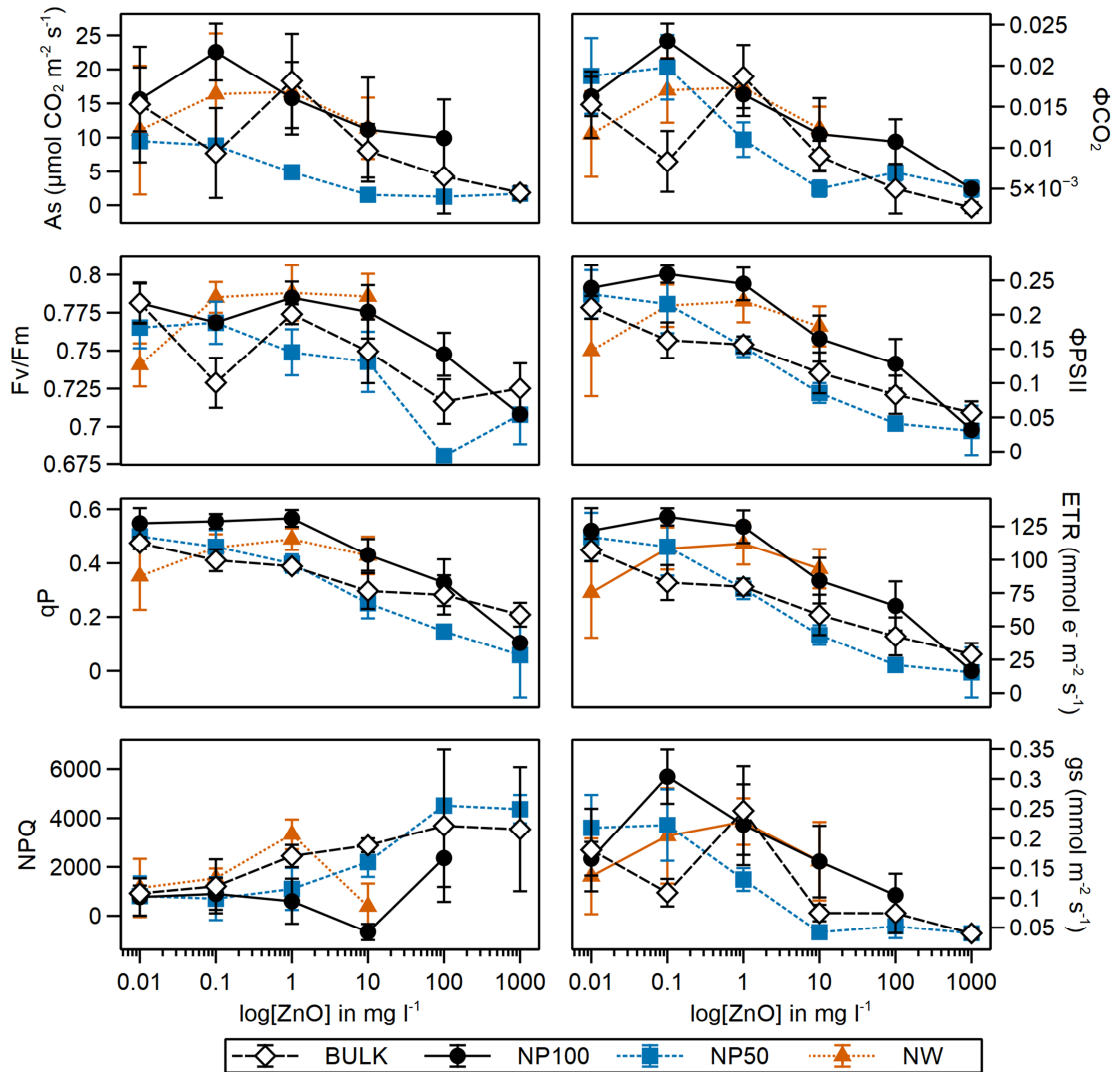


Fig. 4. Photosynthetic performance under ZnO stress. Plants were treated with four different ZnO sources: micron-size (Bulk), NP < 100 nm (NP100), NP < 50 nm (NP50), and nanowires of 50 nm diameter (NW). Data represent means \pm SE, where n = 4. The variables Fv/Fm (maximum quantum yield of PSII photochemistry), Φ PSII (quantum yield of PSII electron transport, qP (photochemical quenching), and NPQ (non-photochemical quenching) are dimensionless.

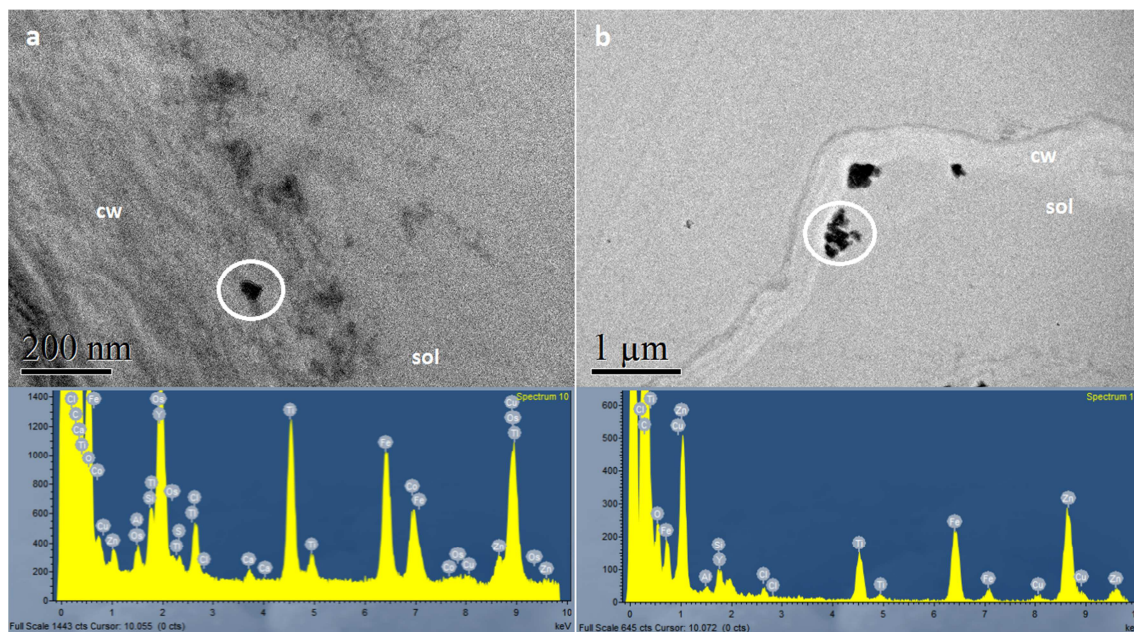


Fig. 5. ZnO-NPs on the root surface. Roots in (a) were treated with NP < 50 nm (NP50), while roots in (b) were treated with NP < 100 nm (NP100). Spectra represent X-Ray spectrometry analysis of the circled areas. Cell wall = cw; exterior solution = sol.

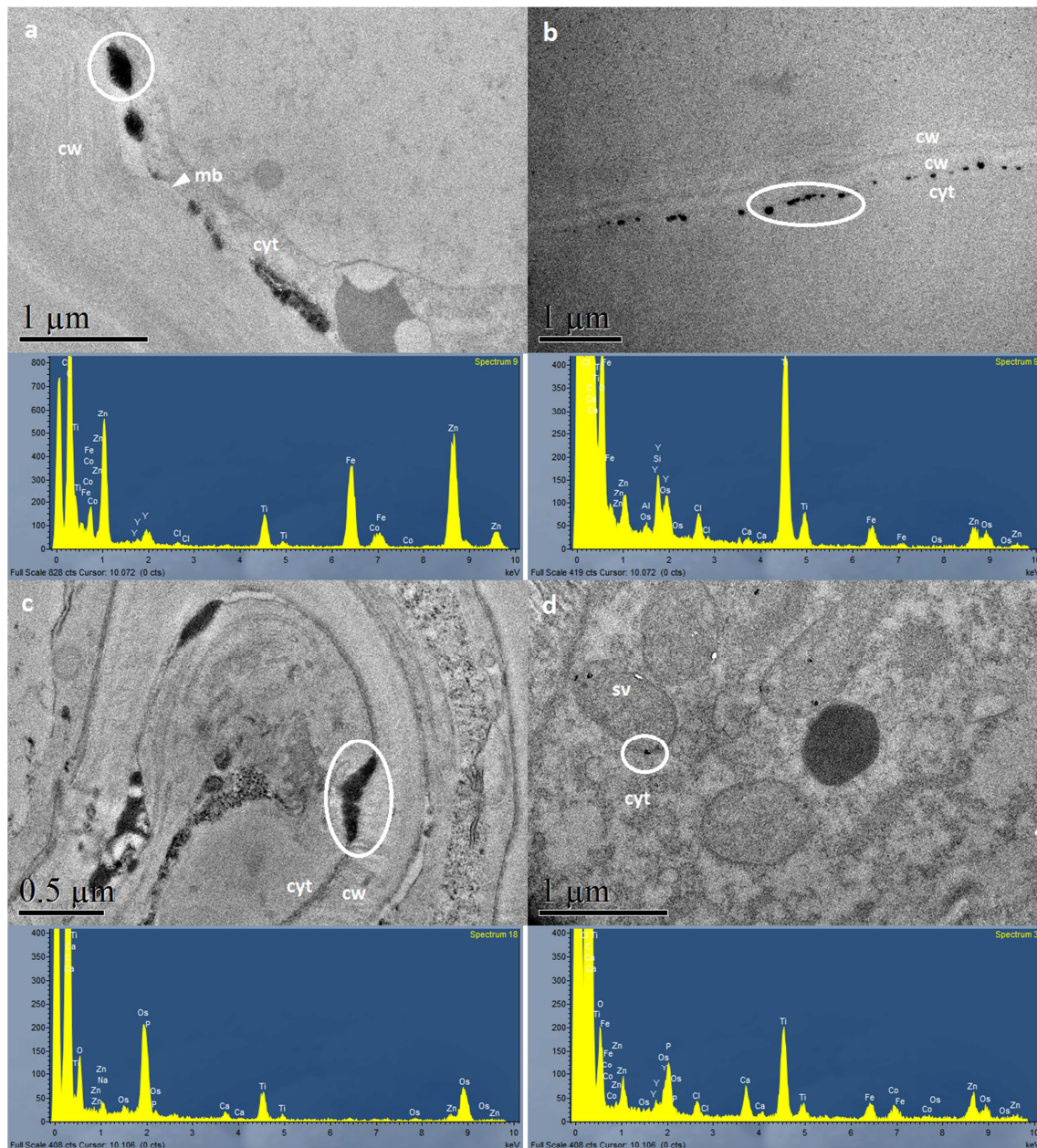
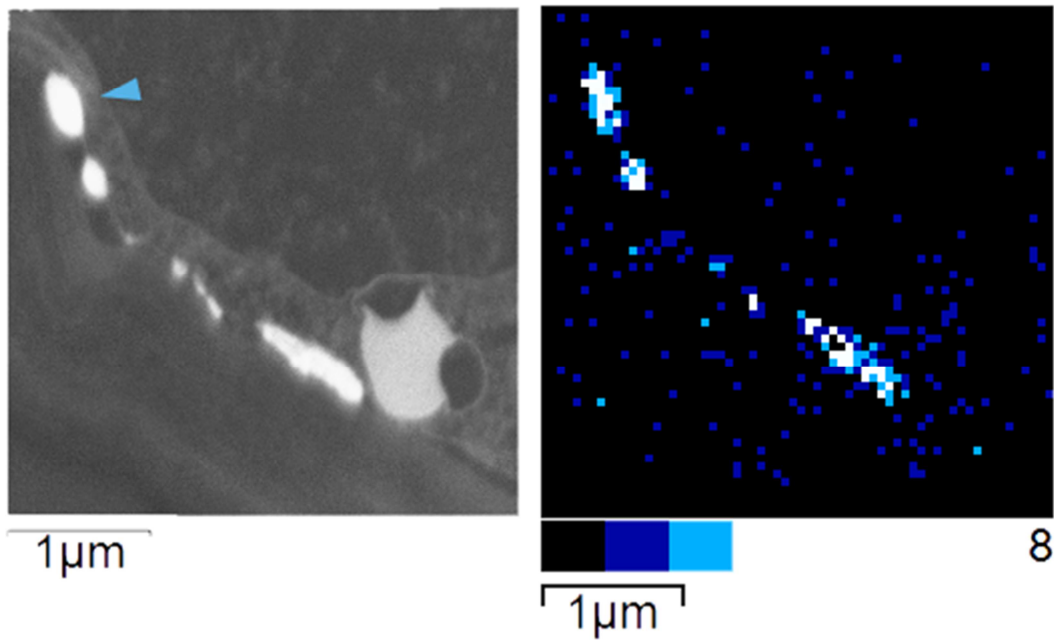


Fig. 6. Zinc deposits in the root cortex. (a), (b), and (c) show Zn precipitates between the cell walls and plasma membranes in NP50, NP100, and Bulk plants, respectively. (d) shows Zn sequestration in small vacuoles in NP50 plants. Spectra represent X-Ray spectrometry analysis of the circled areas. Cell wall = cw; cytoplasm = cyt; plasma membrane = mb; small vacuole = sv.

851



852

853 Fig. 7. Dark-field micrograph and elemental map of the same region as Fig.6a. The Zn
854 precipitates were located between the cell walls and plasma membranes in the NP50 root cortex.
855 The colour scale indicates the intensity of the Zn signal in counts, from 0 (black) to 8 (white).

856